Spatially resolved photoluminescence and Raman mapping of epitaxial GaN laterally overgrown on sapphire

J.-S. Song,[1] H. Rho,[1,*] M. S. Jeong,[2] J.-W. Ju,[3] and I.-H. Lee[3]
[1]*Department of Physics, Research Institute of Physics and Chemistry, Chonbuk National University, Jeonju 561-756, Korea*
[2]*Advanced Photonics Research Institute, Gwangju Institute of Science and Technology, Gwangju 500-712, Korea*
[3]*School of Advanced Materials Engineering, Chonbuk National University, Jeonju 561-756, Korea*
(Received 26 April 2010; revised manuscript received 28 May 2010; published 21 June 2010)

We report spatially resolved photoluminescence (PL) and micro-Raman scattering studies of epitaxial lateral overgrowth (ELO) of GaN on a SiO_2-masked sapphire substrate. Near-field scanning optical microscope measurements show that the ELO layers exhibit strong band-edge emission and yellow-band emission. Raman spectra reveal E_2 (low) and E_2 (high) phonon modes at $\sim$143 and $\sim$569 cm^{-1}, respectively. Interestingly, the E_2 (high) phonon intensity is significantly increased in the ELO layers. Furthermore, minima of the spectral widths of this mode occur in the ELO layers. The E_2 (low) phonon mode exhibits similar behavior, that is, its intensity is stronger in ELO GaN on SiO_2 stripes than in coherently grown GaN on the mask openings. PL and Raman results suggest that crystalline quality is enhanced and threading dislocation density is reduced in the ELO layers.

DOI: 10.1103/PhysRevB.81.233304 PACS number(s): 78.30.Fs, 78.55.Cr

In order to maximize the emission efficiency of GaN through improvement of crystalline quality, the reduction of threading defects is crucial. Among efforts to reduce threading dislocation density, the epitaxial lateral overgrowth (ELO) technique has been widely utilized.[1] When an epitaxial GaN layer is laterally overgrown on a dielectric mask, such as SiO_2 or SiN, the threading dislocation density can be significantly reduced, resulting in enhanced emission efficiency.[2,3] In this technique, a mask layer is typically patterned on top of a GaN template layer grown on a sapphire substrate. The ELO GaN structure thus consists of two regions, including a laterally grown "wing" region over the mask surface and a vertically (or coherently) grown "window" region over the mask opening. ELO layers are overgrown laterally from the outer boundary edges of each mask stripe and coalesce at the centers of the stripes. Threading defects may be generated at the coalesced boundaries (or meeting fronts), with consequent deterioration in emission efficiency.[2] Although the threading dislocation density of laterally grown GaN can be reduced, the presence of the underlying mask pattern induces differences in crystalline quality and stress between the wing and widow regions. The ELO GaN structure, therefore, suffers intrinsically from spatial variations in emission efficiency related to spatial inhomogeneities in crystalline quality and stress.[2–5] Modified techniques, such as the pendeoepitaxial lateral overgrowth technique, have been proposed for enhanced material quality. However, GaN layers grown using this technique also exhibit spatial variations in stress.[6] To investigate crystalline quality and stress in the ELO GaN structure in detail, high-resolution spatial mapping may be performed over the sample surface. In this study, we report spatially resolved photoluminescence (PL) and micro-Raman scattering results for mapping the spatial variations in emission efficiency, crystalline quality, and stress in the ELO GaN structure.

An ELO GaN structure was grown by metal organic chemical vapor deposition. A 100-nm-thick SiO_2 film was deposited onto the GaN buffer layer grown on a (0001)-oriented sapphire substrate; the SiO_2 film was then patterned into 12-μm-wide mask stripes oriented along the $[1\bar{1}00]$ direction using a standard photolithography technique. Openings in the window regions between stripes were 4 μm wide. Finally, a 9-μm-thick GaN layer was grown on top of the patterned surface, resulting in an ELO layer over the SiO_2 mask stripes and a coherently grown layer over the mask openings. PL imaging measurements using a near-field scanning optical microscope (NSOM) were performed at room temperature using a computer-controlled piezo-stage over an area of 50×50 μm^2. The top surface of the sample was excited in the near field using a 325-nm He-Cd laser through a tapered optical fiber tip with a 100-nm aperture.

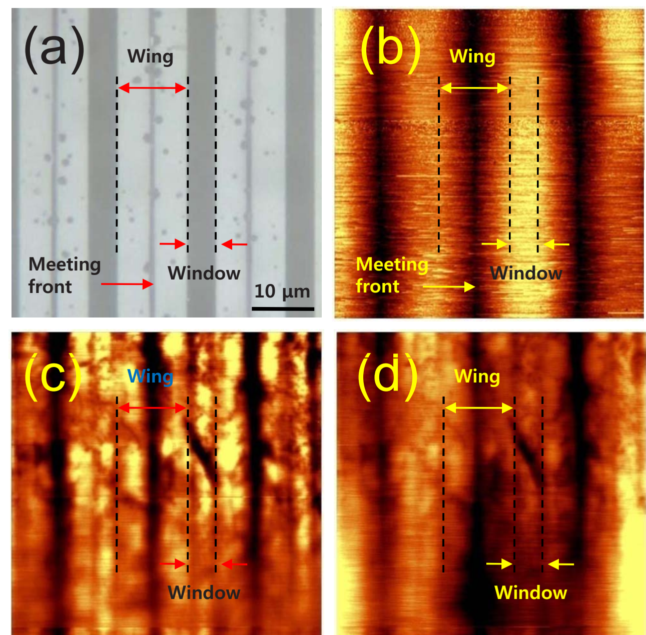

FIG. 1. (Color online) (a) Optical microscope image of the sample surface. (b) NSOM topography image. (c) PL image of the near band-edge emission. (d) PL image of the yellow-band emission.

 ©2010 The American Physical Society

The emitted light was collected from the opposite side of the sample using a high-numerical aperture 40× microscope objective. Micro-Raman line-scan measurements were performed above the sample surface along the direction perpendicular to the SiO_2 stripe orientation at room temperature in a backscattering geometry. A 632.8-nm He-Ne laser was used to excite the sample surface through an optical microscope with a spatial resolution better than 1 μm. The sample was placed on a computer-controlled piezo-stage that was moved 60 μm across the stripes in 500-nm intervals. Scattered light from the sample was dispersed through a monochromator using a 150 grooves/mm grating (for PL measurements) or a 2400 grooves/mm grating (for micro-Raman measurements) and was detected using a thermoelectrically cooled charge-coupled device detector.

Figure 1(a) shows an optical microscope image (50×50 μm^2) of the top surface of the sample. The bright and dark bands correspond, respectively, to the wing and window regions. The narrow dark lines at the center of the wing regions correspond to the meeting fronts of the ELO layers and separate each wing region into two parts, i.e., the left and right wings. Figure 1(b) shows the NSOM topography image, corresponding to the area shown in the optical microscope image. The color shading depicts topographic height change, with darker colors for troughs and brighter colors for crests. The surface topography image exhibits a periodic undulation in height perpendicular to the SiO_2 stripe orientation, with grooves at the meeting fronts of the wing regions and crests at the center of the window regions. The height difference between grooves and crests is approximately 100 nm, corresponding to the thickness of the SiO_2 stripes.

Figures 1(c) and 1(d) show the NSOM images obtained simultaneously with the topography image in Fig. 1(b). The images display PL integrated intensity mappings of near band-edge emission and yellow-band emission, respectively. The band-edge emission shown in Fig. 1(c) is quite strong in both the ELO GaN regions and the coherently grown GaN regions. In contrast, the band-edge emission is considerably weaker at the meeting fronts and at the boundary edges of the SiO_2 mask stripes. The average PL intensity of band-edge emission in the wing regions is similar to that in the window regions. The overall trend of the intensity image for the yellow-band emission is nearly the same as that for the band-edge emission. Our results demonstrate that nonradiative recombination centers attributable to causes such as threading defects are not fully responsible for the yellow luminescence. Similar luminescence behaviors can also be observed via cathodoluminescence measurements on the ELO GaN structure, in which yellow luminescence does not originate from dislocations.[2]

Boundary edges of the SiO_2 mask stripes (i.e., interfaces between wing and window regions) are clearly identified by weak emission intensities, represented by dark lines, in Figs. 1(c) and 1(d). X-ray diffraction measurements reveal that wing tilt of a few degrees occurs in ELO GaN on the SiO_2 mask stripes, increasing defect densities at wing-window transition regions.[7] The topography image shown in Fig. 1(b) exhibits a curved surface morphology with grooves at the meeting fronts, suggesting that the c axis of laterally grown GaN in the wing regions is tilted with respect to the perfect direction. Therefore, reductions in PL efficiency at the wing-window boundaries, as shown in Figs. 1(c) and 1(d), are mostly due to defects associated with the crystalline tilt. Interestingly, the emission efficiencies of both band-edge and yellow luminescence are considerably weakened at the meeting fronts. Transmission electron microscope (TEM) studies reveal that dislocations related to the misorientation of tilted wings are created at the meeting fronts.[8,9] Defects generated over the center regions of the SiO_2 mask are, therefore, responsible for the dramatic reduction in emission efficiency.

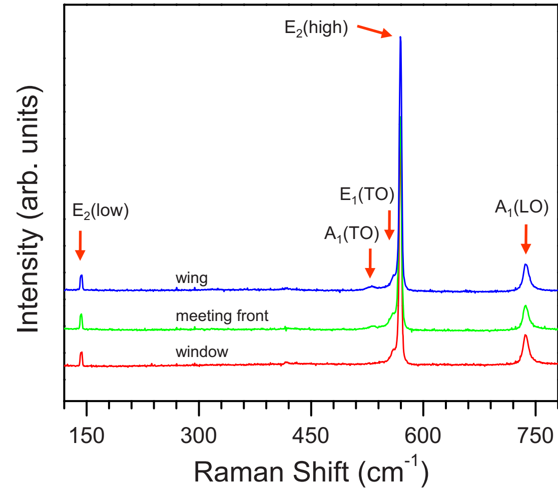

FIG. 2. (Color online) Representative Raman spectra obtained from wing, wing center (i.e., meeting front), and window regions.

In order to investigate spatial variations in stress and crystalline quality in the ELO GaN structure, we performed micro-Raman line-scan measurements. Figure 2 shows representative Raman spectra extracted from the wing and window regions. The Raman spectra reveal sharp E_2 (low) and E_2 (high) phonon modes at ~143 and ~569 cm^{-1}, respectively, and a broad A_1 (LO) phonon mode at ~737 cm^{-1}. The E_2 (low) [E_2 (high)] phonon mode is mostly involved with the vibration of Ga (N) atoms in opposite directions in the basal plane; the A_1 (LO) phonon mode corresponds to the normal mode along the c axis.[10,11] These phonons are symmetry allowed in a backscattering geometry along the c axis of a wurtzite GaN single crystal structure (space group $P6_3mc$-C_{6v}^4). In addition, relatively weak symmetry-forbidden A_1 (TO) and E_1 (TO) phonon modes are observed at ~532 and ~559 cm^{-1}, respectively. The A_1 (TO) phonon mode is observed only in the wing regions including the meeting fronts. The observation of the A_1 (TO) phonon mode is mostly attributed to the slight deviation of the backscattering geometry due to bending of the wings.

A spatial mapping of the E_2 (high) phonon mode provides useful information on crystalline quality and stress in the ELO GaN structure. Figure 3(a) shows an intensity map of the E_2 (high) phonon mode along the direction perpendicular to the SiO_2 stripe orientation. The line-scan data are displayed in a false-color image, with hues ranging from blue for the background to red for the highest intensity. The contrast in intensity between the wing and window regions is clearly visible. The intensity plot of the E_2 (high) phonon mode exhibits several distinctive features: (i) enhanced in-

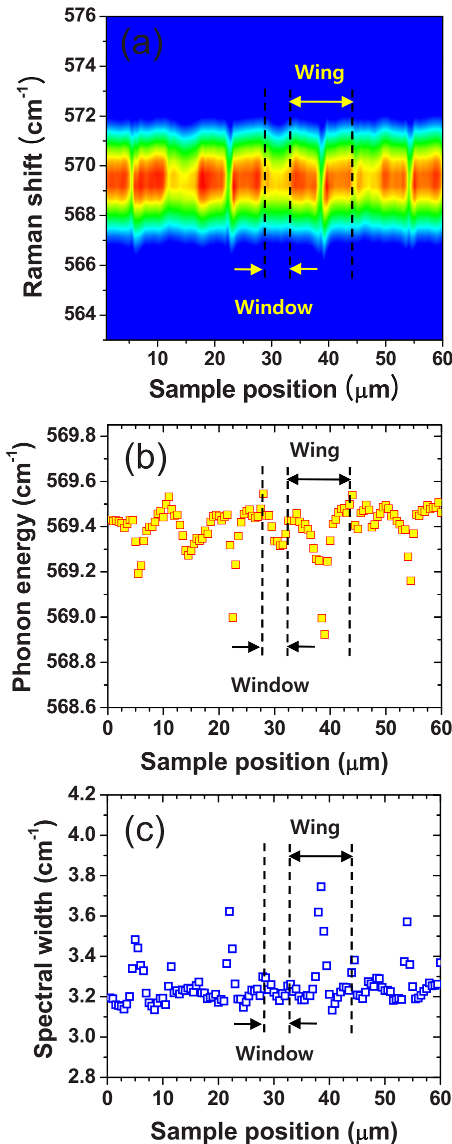

FIG. 3. (Color online) (a) Raman line-scan intensity plot of the E_2 (high) phonon mode across the SiO_2 stripes. (b) E_2 (high) phonon energy changes as a function of the sample position. (c) E_2 (high) phonon linewidth changes as a function of the sample position.

tensities in the ELO layers, (ii) dramatically decreased intensities at the meeting fronts, and (iii) downward shifts of the E_2 (high) phonon energy at the meeting fronts. The intensity of the E_2 (high) phonon is stronger in the wing regions by approximately 15% than that in the window regions. The enhancement of E_2 (high) phonon intensity indicates that crystalline quality is better in the wing regions than in the window regions, suggesting a reduction in threading dislocation density in the ELO layers.[12] The distinctive contrast in intensities between the wing and window regions demonstrates that the E_2 (high) phonon mode is quite sensitive to spatial variations in crystalline quality. Similar to the NSOM data, in which average PL intensity is considerably weakened at the meeting fronts, minima in the intensities of the E_2 (high) phonon mode also occur at the meeting fronts; these minima are approximately 10% weaker than the intensities seen in the window regions. TEM measurements show that dislocations were more prominent at the coalescence fronts than at the boundary edges of mask stripes.[8] Therefore, the diminished E_2 (high) phonon intensities at the meeting fronts are mostly due to defects associated with dislocations and crystallographic imperfection.[4]

To extract values for energies and spectral widths, individual E_2 (high) phonon modes were fitted to a Lorentzian line shape. Figure 3(b) shows that, compared to the bulk value of 567.6 cm^{-1} at room temperature,[10] all of the peak values are shifted upward, indicating that the GaN layer is compressively stressed, as expected in GaN grown on sapphire substrates.[4] Maxima in the peak values occur at the boundary edges between wing and window regions. At the same time, as shown in Fig. 3(c), the spectral widths are broadened, though weakly, at the wing-window boundaries. The increased peak values and the broadened spectral widths at the wing-window boundaries are mostly due to accumulated strain and crystallographic imperfection in the GaN over the SiO_2 stripe edges. The E_2 (high) phonon energy is gradually shifted downward by -0.2 cm^{-1} from the wing-window boundaries to the centers of the window regions, where spectral widths become slightly narrower. Minima in the spectral widths of the E_2 (high) phonon mode occur in the ELO layers. This narrower spectral width indicates better crystalline quality in the ELO GaN than that in the coherently grown GaN, consistent with the increase in the Raman intensity in the GaN wings. Interestingly, along with significant broadening of the spectral widths, a dramatic decrease in the E_2 (high) phonon energy is observed at the meeting fronts. Specifically, the E_2 (high) phonon energy decreases by -0.5 cm^{-1}, indicating a relaxation of strain at the meeting fronts.

In general, Si doping induces relaxation of compressive strain in GaN, resulting in a downward shift in the E_2 (high) phonon energy.[13] The significant relaxation of strain toward the meeting fronts may be attributed to the additional doping caused by incorporation of Si atoms into growth fronts during the lateral growth of GaN on the top surfaces of the SiO_2 stripes.[5] The LO phonon-plasmon coupled mode can evolve with doping, resulting in an asymmetric line shape of the A_1 (LO) phonon mode.[5] In our measurements, however, there are no noticeable changes in the peak energies and line shapes of the A_1 (LO) phonon mode in any of the line-scan data throughout the sample surface. For instance, the A_1 (LO) phonon modes of the Raman spectra shown in Fig. 2 exhibit almost the same line shapes and do not demonstrate any additional scattering associated with the LO phonon-plasmon coupled mode. Thus, the effect of Si doping on the downward shifts of the E_2 (high) phonon energies near the meeting fronts is negligible.

Strain related to dislocations is often tensile. Therefore, we argue that the relaxation of strain due to the increase in dislocation density accumulated near the meeting fronts results in a decrease in the E_2 (high) phonon energy. Under a biaxial assumption in the basal plane, $\varepsilon_c=3.8\times10^{-4}\Delta\omega$ and $\varepsilon_c/\varepsilon_a=-0.6$, where ε_c and ε_a are strains along the c and a axes of GaN, respectively, and $\Delta\omega$ is the E_2 (high) phonon energy shift.[14] The in-plane biaxial stress related to ε_c is calculated to be $\sigma_a=-630.4\varepsilon_c$ GPa.[14] Therefore, the E_2

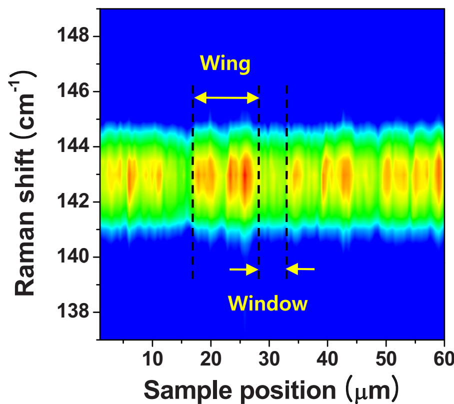

FIG. 4. (Color online) Raman line-scan intensity plot of the E_2 (low) phonon mode across the SiO_2 stripes.

(high) phonon energy difference of $\Delta\omega=0.5\ \text{cm}^{-1}$ between the meeting fronts and other regions corresponds to an in-plane strain difference of $\Delta\varepsilon_a=0.0003$ and an in-plane stress difference of $\Delta\sigma_a=0.12$ GPa.

The directions of the crystallographic tilting angles are in opposition at the meeting fronts, leading to inhomogeneous distribution of strain.[8,9] We argue that crystallographic imperfection and complicated strain field due to the misalignment of ELO layers at the meeting fronts are represented by significant broadening in the spectral widths of the E_2 (high) phonon mode. Doping-induced structural disorder can also cause broadening in spectral widths; however, the effect of doping on the linewidth broadening near the meeting fronts is negligible, since there is no signature of the A_1 (LO) phonon-plasmon coupled mode associated with doping.

Figure 4 shows the intensity mapping of the E_2 (low) phonon mode across the SiO_2 mask stripes. The overall intensity profile of the E_2 (low) phonon mode is similar to that of the E_2 (high) phonon mode, i.e., stronger in the wing regions than in the window regions. Also, the E_2 (low) phonon response is considerably weakened at the meeting fronts. Interestingly, the E_2 (low) phonon intensities are stronger near the outer edges of each of the left and the right wings, i.e., in the regions near the SiO_2 stripe edges and near the meeting fronts. The enhancement in the E_2 (low) phonon intensity is presumably due to refraction and increased scattering rate of the excitation light related to the dislocations created near the stripe edges and near the meeting fronts.[5] The E_2 (high) phonon mode also shows similarly enhanced intensities near the outer edges of each of the left and right wings.

In summary, we performed spatially resolved PL and micro-Raman scattering measurements on an ELO GaN structure. The overall profile of the yellow-band emission is similar to that of the band-edge emission, suggesting that dislocations are not the origin of the yellow-band emission. Crystalline quality is enhanced in the ELO GaN layer, as evidenced by increased E_2 (high) and E_2 (low) phonon intensities. Crystalline imperfection and dislocations at the meeting fronts are attributed to the dramatic reductions in both PL intensity and E_2 phonon intensity. The relaxation of stress and the broadening of spectral widths are observed at the meeting fronts. Our results demonstrate that spatially resolved micro-Raman scattering, together with spatially resolved PL, can provide comprehensive understanding of crystalline quality and stress distributions in an ELO GaN structure.

This research was supported by Basic Science Research Program through the National Research Foundation of Korea (NRF) funded by the Ministry of Education, Science and Technology (Grants No. 2009-0074315 and No. 2009-0089501) and by Nano R&D program through the Korea Science and Engineering Foundation funded by the Ministry of Education, Science and Technology (Grant No. 2007-02939). Sample growth was supported by the Korea Research Foundation Grant funded by the Korean Government (MOEHRD) (Grant No. KRF-2007-521-D00296). H. R. thanks H. Jeong for technical help in the use of the NSOM facility.

*rho@chonbuk.ac.kr

[1] P. Gibart, Rep. Prog. Phys. **67**, 667 (2004).
[2] S. Dassonneville, A. Amokrane, B. Sieber, J.-L. Farvacque, B. Beaumont, and P. Gibart, J. Appl. Phys. **89**, 3736 (2001).
[3] J. C. Moore, V. Kasliwal, A. A. Baski, X. Ni, Ü. Özgür, and H. Morkoç, Appl. Phys. Lett. **90**, 011913 (2007).
[4] M. Kuball, M. Benyoucef, B. Beaumont, and P. Gibart, J. Appl. Phys. **90**, 3656 (2001).
[5] V. V. Chaldyshev, F. H. Pollak, M. Pophristic, S. P. Guo, and I. Ferguson, J. Appl. Phys. **92**, 6601 (2002).
[6] U. T. Schwarz, P. J. Schuck, M. D. Mason, R. D. Grober, A. M. Roskowski, S. Einfeldt, and R. F. Davis, Phys. Rev. B **67**, 045321 (2003).
[7] N. Gmeinwieser, K. Engl, P. Gottfriedsen, U. T. Schwarz, J. Zweck, W. Wegscheider, S. Miller, H.-J. Lugauer, A. Leber, A. Weimar, A. Lell, and V. Härle, J. Appl. Phys. **96**, 3666 (2004).
[8] A. Sakai, H. Sunakawa, and A. Usui, Appl. Phys. Lett. **73**, 481 (1998).
[9] Z. R. Zytkiewicz, J. Z. Domagala, D. Dobosz, L. Dobaczewski, A. Rocher, C. Clement, and J. Crestou, J. Appl. Phys. **101**, 013508 (2007).
[10] V. Yu. Davydov, Yu. E. Kitaev, I. N. Goncharuk, A. N. Smirnov, J. Graul, O. Semchinova, D. Uffmann, M. B. Smirnov, A. P. Mirgorodsky, and R. A. Evarestov, Phys. Rev. B **58**, 12899 (1998).
[11] H. Harima, J. Phys.: Condens. Matter **14**, R967 (2002).
[12] Geometrical effects, such as tilted surface topography, and/or material volume change under excitation may also contribute to spatial variations in the E_2 (high) phonon intensity.
[13] Z. Chine, A. Rebey, H. Touati, E. Goovaerts, M. Oueslati, B. El Jani, and S. Laugt, Phys. Status Solidi A **203**, 1954 (2006).
[14] C. Kisielowski, J. Krüger, S. Ruvimov, T. Suski, J. W. Ager III, E. Jones, Z. Liliental-Weber, M. Rubin, E. R. Weber, M. D. Bremser, and R. F. Davis, Phys. Rev. B **54**, 17745 (1996).